Chem. Res. Chinese Universities, 2020, 36(1), 68—73 doi: 10.1007/s40242-019-0040-3

Article

Controllable Synthesis of Hollow Multishell Structured Co_3O_4 with Improved Rate Performance and Cyclic Stability for Supercapacitors

WANG Cong[1,2], WANG Jiangyan[1], HU Wenping[2] and WANG Dan[1*]

1. State Key Laboratory of Biochemical Engineering, Institute of Process Engineering, Chinese Academy of Sciences, Beijing 100190, P. R. China;

2. Department of Chemistry, School of Science & Collaborative Innovation Center of Chemical Science and Engineering, Tianjin University, Tianjin 300072, P. R. China

Abstract Hollow multishelled structures(HoMSs) Co_3O_4 with specially appointed shell number(double-, triple- and quadruple-) were accurately prepared by a sequential templating approach. Due to the superiorities of inimitable porous multishelled structure, triple-HoMSs Co_3O_4 achieved the best performance among all the samples with a specific capacitance of 1028.9 F/g at 10 mV/s and 688.2 F/g at 0.5 A/g, respectively. Furthermore, the electrode delivered a high rate performance(89.8% retention at 10 A/g) and excellent cycle stability(6.8% loss over 2000 cycles), showing a great promise for practical application in the future.

Keywords Hollow multishelled structure; Cobalt oxide; Supercapacitor

1 Introduction

With the deterioration of the atmosphere environment and urgency needed for renewable sources, supercapacitors(SCs), combing the advantages of lithium ion batteries and conventional capacitors, have been broadly used in various fields as new energy conversion and storage devices in recent few decades[1—4]. Among different kinds of electrode materials, transition metal oxides, which can realize efficient redox charge transfer by changing the valence of transition metal elements are deemed to ideal electrode materials for pseudocapacitors[5—9]. Particularly, cobalt oxides(such as Co_3O_4) with high theoretical specific capacitance, good thermal stability and high redox activity, are considered as promising electrode materials[10,11]. However, there are still many shortcomings restricting their further applications in supercapacitors; for instance, poor electronic conductivity(giving rise to specific capacitance declining in fast redox reaction), and destruction and collapse of micro structure during charge and discharge process(causing poor cycle stability)[1,12,13].

To overcome these shortcomings, one effective approach is to synthesize and assemble active electrode materials with controllable micro-structures and sizes, possessing beneficial physical and chemical properties superior to those of the bulk materials[14,15]. Porous hollow nanostructures have caused widespread concern because they can facilitate electrolyte permeating to bulk and provide shorter transport paths for both electrolyte ions and electrons, resulting in reduced internal resistance and improved high-rate performance[16—20]. Especially, hollow multishelled structures(HoMSs) are superior to the above involved hollow structures with single shell in the light of the following aspects[21,22]: (1) more fully utilizing hollow space inside can not only maintain free volume of the cavity, but also improve contact area between electrode and electrolyte; (2) possessing better structure stability during redox reaction owing to the adjacent shells supporting each other. For example, septuple-HoMSs$(Co_{1-x}Mn_x)(Co_{1-y}Mn_y)_2O_4$[23] and quadruple-HoMSs Mn_2O_3[24] exhibited outstanding electrical performance applied in SCs. Therefore, the HoMSs as SCs active materials may effectively improve the specific capacitance, rate capability, as well as cycling stability.

Recently, various processes have been explored to synthesize multishelled structure. Kang *et al.*[25] have synthesized Co_3O_4 HoMSs using spray drying techniques. In Wang's group[26—31], a series of transition metal oxide-based HoMSs has been extensively reported by a sequential templating approach(STA) using carbonaceous microspheres(CMSs) as templates. According to this universal and low-cost approach, earth abundant metal oxide HoMSs should be promising candidates as the electrode materials of SCs with large capacitance and good rate capability.

Herein, based on the previous works in our group[27], precisely controlled double-(2S-), triple-(3S-) and quadruple-(4S) HoMSs Co_3O_4 were synthesized through STA. Owing to the unique multi-layered hierarchical structure, 3S-HoMSs Co_3O_4 exhibited significantly improved charge storage capability with

*Corresponding author. Email: danwang@ipe.ac.cn

Received November 8, 2019; accepted December 3, 2019.

Supported by the National Natural Science Foundation of China(Nos.21590795, 21821005, 51772296, 51772294, 51702321, 51972306, 51802306).

specific capacitances of 1028.9 and 688.2 F/g at a scan rate of 10 mV/s and a current density of 0.5 A/g, respectively. Furthermore, the high power made it an even greater promise in practical application.

2 Experimental

2.1 Synthesis of HoMSs Co_3O_4

HoMSs Co_3O_4 nanoparticles were synthesized with some modification through a hard-template method. CMSs as sacrificial hard templates were synthesized by the hydrothermal polymerization reaction of sucrose. Firstly, 1.5 mol/L sucrose aqueous solution was dissolved completely. Next, the autoclaves with solution were heated at 200 °C for 2 h. The resulting suspension was washed with deionized water several times, and then dried in oven. Afterwards, the synthesis of the 4S-HoMSs Co_3O_4 was used as an example to describe the formation process. Freshly-prepared CMSs(0.4 g) were dispersed in 20 mL of 0.8 mol/L cobalt acetate solution[V(water):V(ethanol)= 1:4] with the continuous stirring and ultra-sonication. Resulting uniform suspension was stirred constantly in a water bath at 30 °C maintaining 6 h to complete the absorption. After that, the resultant CMSs with cobalt salt were heated in a muffle furnace. The programming heating process is holding the rate of 1 °C/min to 500 °C and then kept for 1 h. After the above process, the 4S-HoMSs Co_3O_4 with high purity were synthesized. Different shell numbers of HoMSs were controlled with changing composition of precursor(detailed experimental parameters can be found in Table S1, see the Electronic Supplementary Material of this paper). Adjusting the concentration of cobalt acetate to 0.2 mol/L with absorption and calcination condition staying the same, single-shelled Co_3O_4 hollow microspheres(1S-HoMSs) and Co_3O_4 nanoparticles(Co-NPs) were obtained.

2.2 Characterization for HoMSs Co_3O_4

The crystallinity of HoMSs Co_3O_4 was determined by powder X-ray diffraction(XRD) with Cu $K\alpha$ radiation(λ, 0.15405 nm). The morphologies of HoMSs Co_3O_4 were observed by scanning electron microscopy(SEM, JSM-6700, operating at 5.0 kV) and transmission electron microscopy (TEM, FEI Tecnai F20, 200 kV). X-Ray photoelectron spectroscopies(XPS) were output by an electron spectrometer (ESCALab220i-XL with 300 W Al $K\alpha$ radiations). The nitrogen absorption-desorption isotherms were measured to obtain pore distribution with a Quantochrome Autosorb-1MP sorption analyzer. The thermo gravimetric analysis-differential thermal analysis(TGA-DTA) data were collected through a DTA-60(Shimadzu, Japan).

2.3 Electrochemical Performance for HoMSs Co_3O_4

We used a three-electrode electrochemical system to evaluate the performance of the synthesized HoMSs Co_3O_4. The mass ratio of HoMSs Co_3O_4:carbon black:polyvinylidence difluoride(PVDF)=7:2:1 was used to fabricate electrodes in uniform slurry with *N*-methyl-2-pyrrolidinone(NMP) solvent. Then the slurry was applied onto a nickel foam current collector(diameter: 1.5 cm). The average mass loading of active materials in the working electrode was 1.05 mg/cm^2. The as-prepared nickel foam(working electrode), a platinum foil(counter electrode) and a Hg/HgO(reference electrode) formed the three electrodes test system in 4 mol/L KOH electrolyte. The cyclic voltammetry(CV) and galvanostatic charge/discharge(GC) curves were measured at room temperature on a CHI 660C(CH Instruments, Inc.) electrochemical workstation.

3 Results and Discussion

3.1 Morphology Characterization of HoMSs Co_3O_4

As described in Scheme 1, the HoMSs were prepared by adjusting the absorption process[32]. The homogeneous CMSs with a size of about 2 μm and lots of organic functional groups, such as hydroxyl, carbonyl, etc.(Fig.S1, see the Electronic Supplementary Material of this paper), endowing them high-absorption capability of metallic ions, were synthesized by the hydrothermal polymerization reaction of sucrose.

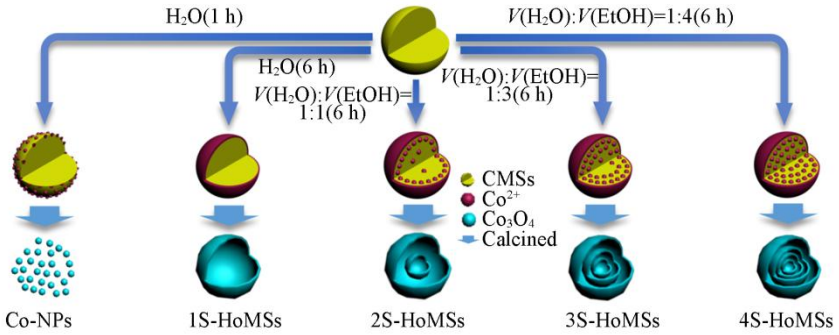

Scheme 1 Synthesis processes for 1S-, 2S-, 3S-, 4S-HoMSs and Co-NPs

Herein, the composition of the precursor solution was essential to control the shell structure of HoMSs under constant calcination conditions. When cobalt acetate aqueous solution was adopted, 1S-HoMSs Co_3O_4 nanoparticles were obtained after the removal of templates by annealing in air at 500 °C for 1 h[Fig.1(A), synthetic details can be found in Table S1]. When 50%(volume fraction) of ethanol was added to the precursor solution, 2S-HoMSs were obtained[as shown in Fig.1(B)] after

the same heating treatment. It could be inferred that absorption capacity of CMSs to cobalt hydrated ions increased with the addition of ethanol by decreasing surface tension of precursor solution and reducing radius of the hydrated cobalt ions[27]. The 3S-HoMSs Co_3O_4 nanoparticals were obtained with the ethanol content increasing to 75%(volume fraction) and the absorption solution heated slightly to 30 °C[Fig.1(C)]. Besides, 4S-HoMSs[Fig.1(D)] can be achieved when the volume ratio of ethanol to water in solvent was increased to 4:1 with other absorption and calcination condition staying the same with that of 3S-HoMSs. In addition, Co_3O_4 nanoparticles(Co-NPs) were obtained(TEM and SEM images shown in Fig.S2, see the Electronic Supplementary Material of this paper) when too few cobalt ions were adsorbed by CMSs to form a shell. As shown in the TEM[Fig.1(A)—(D)] and SEM images(Fig.S3, see the Electronic Supplementary Material of this paper), 1S-, 2S-, 3S- and 4S-HoMSs were uniform with a similar mean size of about 1.0 μm. Moreover, as shown in SEM image[Fig.1(E)], many drapes can be clearly observed on each shell of 3S-HoMSs, which may improve the supercapacitor performance by providing more active sites and enhancing the contact of surfaces. The high-resolution TEM(HRTEM) image[Fig.1(F)] with clear marked (111) and (311) lattice planes of cubic Co_3O_4, respectively, revealed that the shells were formed by the accumulation of nanocrystals. Compared to 1S-HoMSs and 2S-HoMSs, with increasing the number of shells, average shell thickness and grain size become smaller. In order to reduce the surface energy, the nanoparticles tend to form folds during the solidification and crystallization process, which may make the shell structure more stable.

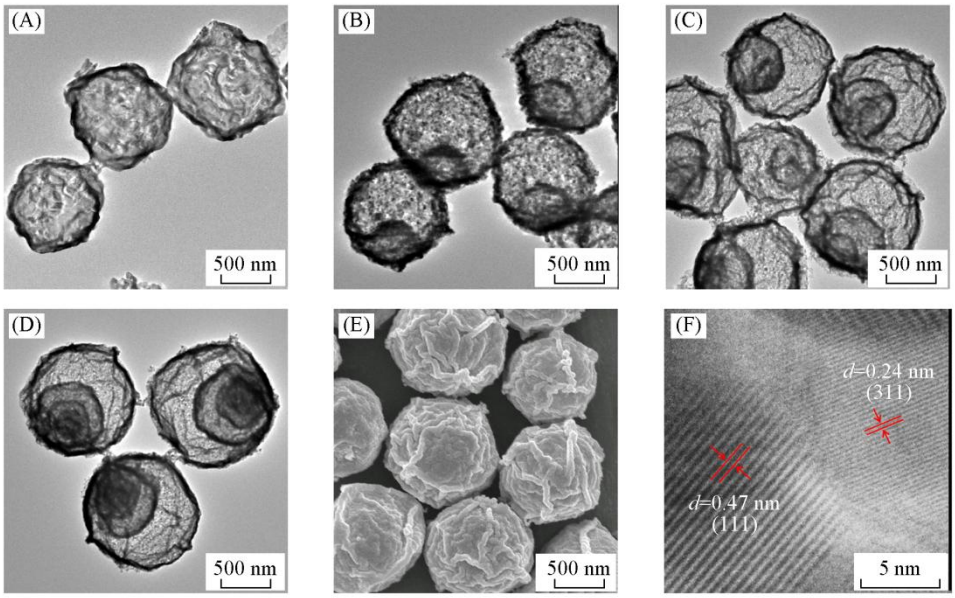

Fig.1 TEM images of 1S-, 2S-, 3S- and 4S-HoMSs(A—D), SEM image of 3S-HoMSs(E) and HRTEM image of partial 3S-HoMSs(F)

3.2 Characterization for HoMSs Co_3O_4

Fig.2(A) showed the crystalline conditions of the as-prepared HoMSs with different shell structures. All the diffraction peaks of the HoMSs were calibrated as pure spinel phase of Co_3O_4(JCPDS No.42-1467), with no impurity peaks detected[33]. The average crystallite diameters of the 1S-, 2S-, 3S- and 4S-HoMSs as well as Co-NPs were calculated to be 29.7, 28.2, 20.9, 21.2 and 21.3 nm, respectively, using the Scherrer equation[34]. The XRD pattern and grain size distribution of Co-NPs were shown in Fig.S4(see the Electronic Supplementary Material of this paper). The average particle size was counted as 20.98 nm. Taking 3S-HoMSs Co_3O_4 as a representative example, the selected area electron diffraction(SAED) pattern[Fig.2(B)] showed distinct concentric rings, which corresponds to the diffraction peaks of the cubic phase of Co_3O_4 from the innermost ring to the outermost, which revealed the polycrystalline nature of the as-prepared HoMSs[14]. Furthermore, XPS was carried out for the investigation of the chemical composition of HoMSs. The energy in the test is based on the binding energy of C_{1s} peak with 284.6 eV[35]. As shown in Fig.2(C), the XPS spectrum of full region indicated the 3S-HoMSs contained only cobalt(Co) and oxygen(O). The O_{1s} spectrum(Fig.S5, see the Electronic Supplementary Material of this paper) of the evaluated sample showed two peaks located at 530 and 531.3 eV [36]. The Co_{2p} spectrum[Fig.2(D)] shows two valence states in the products. Two main peaks of $Co^{3+}_{2p_{3/2}}$ and $Co^{3+}_{2p_{1/2}}$ at 780.1 and 795.1 eV can be observed, separated by 15 eV[32]. Those of $Co^{2+}_{2p_{3/2}}$ and $Co^{2+}_{2p_{1/2}}$ were located at 781.8 and 796.8 eV, respectively[34]. These spectra are fully consistent with the reported data of pure Co_3O_4 phase. The TGA-DTA data(Fig.S6, see the Electronic Supplementary Material of this paper) revealed that the calcination is complete before 305 °C approximately. It was worth noting that the CMSs infused with Co-precursor were annealed at 500 °C for 1 h in order to improve the crystallinity[37].

3.3 Electrochemical Properties for HoMSs Co_3O_4

Fig.3(A) showed the cyclic voltammetry(CV) curves of 3S-HoMSs electrodes over scan rates of 5—100 mV/s in 4 mol/L KOH electrolyte within a window of 0.1—0.6 V(*vs.* Hg/HgO). Meanwhile, the as-prepared electrodes assembled by

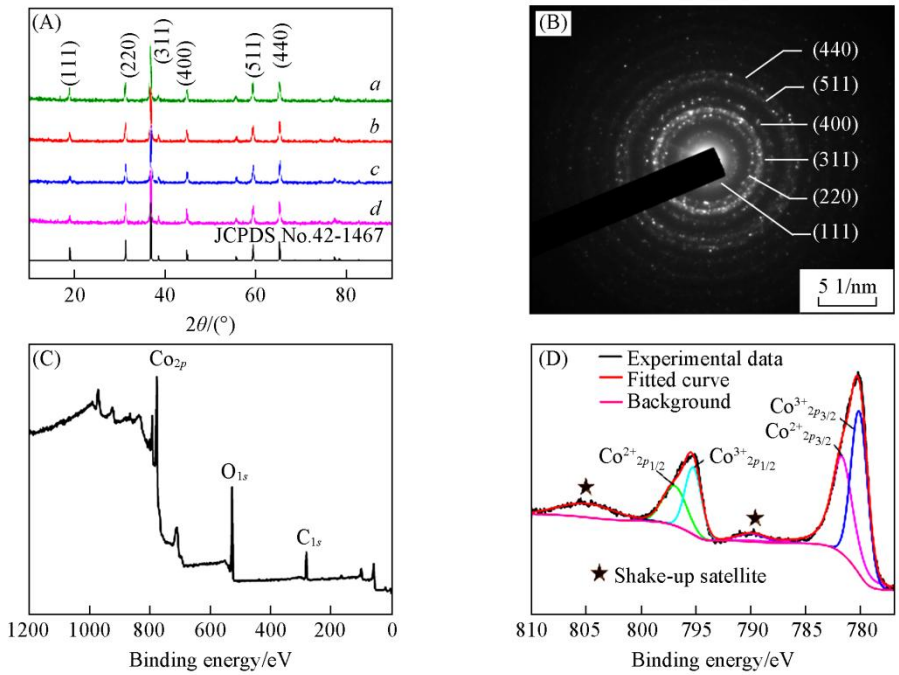

Fig.2 XRD patterns of the as-prepared HoMSs(A), and SAED image(B), high-resolution XPS spectra of full region(C) and Co_{2p}(D) of 3S-HoMSs

(A) *a*—*d*. 1S-, 2S-, 3S- and 4S-HoMSs.

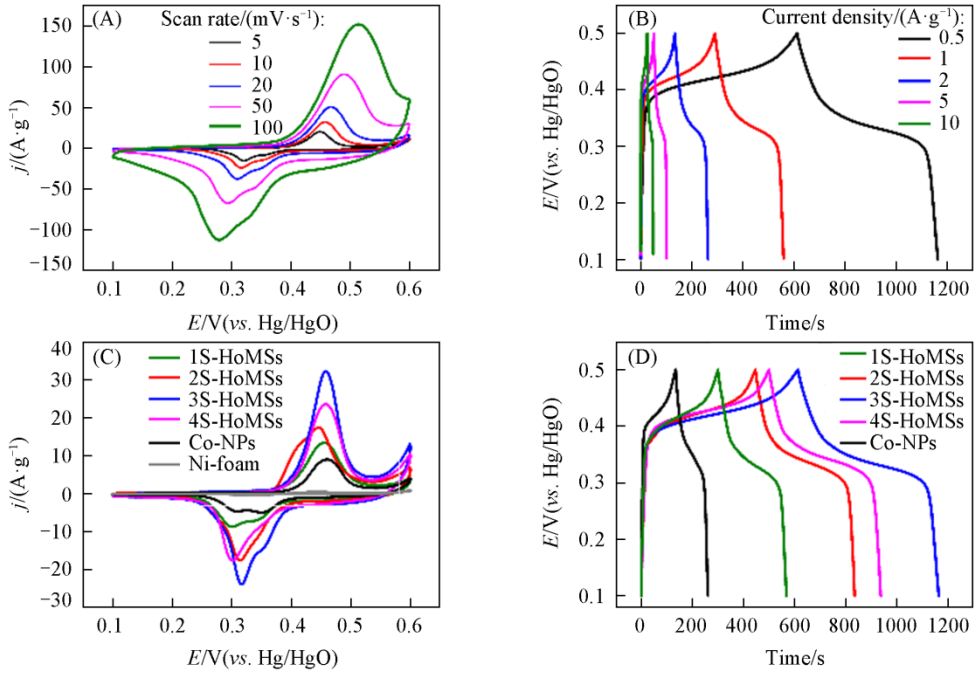

Fig.3 CV curves of 3S-HoMSs at different scan rates of 5, 10, 20, 50 and 100 mV/s(A), galvanostatic charge/discharge curves of 3S-HoMSs at various current densities of 0.5, 1, 2, 5 and 10 A/g(B), comparison of CV curves(C) and galvanostatic charge/discharge curves(D) of 1S-, 2S-, 3S-, 4S-HoMSs and Co-NPs at a scan rate of 10 mV/s and a current density of 0.5 A/g

1S-, 2S-, 3S- and 4S-HoMSs and Co-NPs were also evaluated under the same test condition(Fig.S7, see the Electronic Supplementary Material of this paper)[38]. Two pairs of broad redox(two separated cathodic peaks and single anodic peak) reaction peaks distorted from symmetrical image were observed in the CV curves without rectangular-like shapes, indicating that the Faradic reaction behaviors contributed mostly to the electrochemical capacitance of the active materials[38,39]. The possible mechanism of the surface redox reaction of HoMSs electrode, corresponding to the obvious redox peaks, may be attributed to the reversible transitions between Co(II/III) and Co(III/IV), expressed as follows[9]:

$$Co_3O_4+OH^-+H_2O \rightleftharpoons 3CoOOH+e^- \quad (1)$$

$$CoOOH+OH^- \rightleftharpoons CoO_2+H_2O+e^- \quad (2)$$

The specific capacitance of the 3S-HoMSs decreased with increasing the current densities calculated from the CV

curve(Fig.S8, see the Electronic Supplementary Material of this paper). This may be due to the insufficient diffusion of hydroxide ions from the electrolyte to the surface of the porous HoMSs at a high current density, resulting in partial lack of a dyadic redox reaction[40]. The specific capacitance was 1028.9 F/g at a scan rate of 10 mV/s and kept 806.9 F/g at a high scan rate of 100 mV/s, which was higher than most of previous reports(Table S2, see the Electronic Supplementary Material of this paper)[18,35,41,42]. Moreover, as the scanning rate increased from 5 mV/s to 100 mV/s, the anode peak moved toward a higher potential and the cathode peak moved toward a lower potential, which illustrated the quasi-reversible nature of the electrochemical system[6]. The excellent electrochemical activity of 3S-HoMSs may be attributed to the unique three-dimensional multishelled microstructure, which can provide more reactive sites and transition highway for electrons and electrolyte ions in electronic/ionic transmission processes. Meanwhile, the galvanostatic charge/discharge curves were tested from 0.5 A/g to 10 A/g under the same potential window of 0.1—0.5 V(*vs*. Hg/HgO). As shown in Fig.3(B), the charge/discharge curves of 3S-HoMSs without obvious IR drop indicated a fast *I-V* response with a small equivalent series resistance, which were also consistent with CV curves[23].

The HoMSs with controllable shell numbers have a great advantage in energy storage[23,24]. The comparison of CV curves of different HoMSs and Co-NPs electrodes was shown in Fig.3(C). It can be seen that the redox reaction peaks of the above prepared electrodes appeared in the same positions at 10 mV/s. Furthermore, it's obvious that the integral area of CV curves of 3S-HoMSs, which represented the ability of charge stored on per mass active material in supercapacitor was the largest among four types of HoMSs and Co-NPs. The comparative investigation with bare Ni foam at the same scan rate revealed the contribution of the collector to the capacity can be neglected. Fig.3(D) illustrated the comparison of GC curves of various electrodes at 0.5 A/g, which agreed well with the trend observed in the CV curves. The specific capacitance of the 3S-HoMSs calculated from the GC curve was 688.2 F/g at a current density of 0.5 A/g, which is higher than that of the 4S-HoMSs(551.3 F/g) and 2S-HoMSs(485.3 F/g)[Fig.4(A)]. What's more, it was two times the specific capacitance of the as-prepared 1S-HoMSs and four fold that of Co-NPs. In addition, the specific capacitance of 3S-HoMSs still maintained a relative high value of 618.0 F/g at 10 A/g, only decreasing by 10.2%, which ranked among the best rate performance compared with previous works(Table S2). Meanwhile, the Coulombic efficiency(η) of the 3S-HoMSs electrode maintained 93%—95% with the current density increasing, indicating good rate performance and good reversibility[41].

As for practical applications in supercapacitors, another aspect of concern is cycling stability of electrode materials[13]. In this work, long cycle lives of the as-prepared HoMSs Co_3O_4 and Co-NPs materials were evaluated by consecutive GC test between 0.1 and 0.5 V in 4 mol/L KOH aqueous electrolyte at 2 A/g. The HoMSs electrodes showed better stability than Co-NPs as shown in Fig.4(B). For instance, the specific capacitance of 3S-HoMSs retained 93.2% of its initial value(641.2 F/g at 2 A/g) after 2000 continuous cycles, while only 74.6% and 70.4% of initial capacitance of Co-NPs and 1S-HoMSs can be maintained under the same condition. After 2000 cycles, the spherical structures of 3S-HoMSs were preserved to the utmost extent, rarely broken balls(Fig.S9, see the Electronic Supplementary Material of this paper). It may be attributed to the adjacent shells supporting each other during the cycling process. Meanwhile, no obvious change of Coulombic efficiency can be found after multiple charging and discharging cycles.

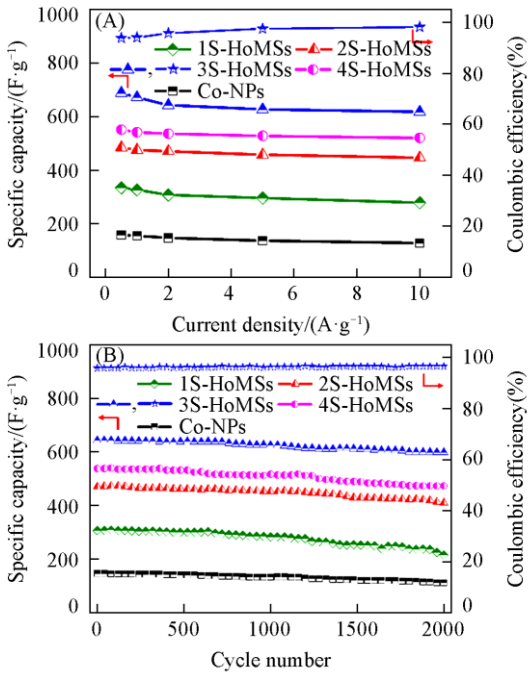

Fig.4 Specific capacitances of 1S-, 2S-, 3S- and 4S-HoMSs and Co-NPs and Coulombic efficiency of 3S-HoMSs at different current densities(A) and cyclic stability of 1S-, 2S-, 3S-, 4S-HoMSs and Co-NPs and corresponding Coulombic efficiency of 3S-HoMSs at a current density of 2A/g(B)

Furthermore, a good understanding of the correlation between the morphology of micro/nanostructure materials and their electrochemical performances is essential to figure out the pseudocapacitor mechanism and develop superior electrode materials of supercapacitors. From the detailed TEM images(Fig.S10, see the Electronic Supplementary Material of this paper), we can find that the average shell thickness of 3S-HoMSs was about 56 nm. It was the thinnest among the various HoMSs, which can be benefited from the smaller grain size and/or fewer grains packing in the shells. As a result, the 3S-HoMSs showed the largest specific surface area of about 22.9 m^2/g[Fig.S11(A), Table S3, see the Electronic Supplementary Material of this paper]. It can be inferred that the smaller the thickness of the shell layer and the larger the specific surface area, the larger the active site and the contact area between the electrode and the electrolyte, thereby obtaining better electrochemical properties[21]. Meanwhile, the Barret-Joyner-Halenda(BJH) pore size distribution curves[Fig.S11(B)] showed that pore sizes of HoMSs Co_3O_4 were mainly distributed between 1 and 10 nm, which could

guarantee the electrolyte to infiltrate into materials. It ensured the redox reactions occurred in adjacent surfaces and full utilization of the electrode material to obtain excellent rate capability[43]. Moreover, due to the supporting of adjacent shells that can alleviate the structural damage caused by swelling and shrinking during redox reaction, HoMSs Co_3O_4 possessed better structural stability and Co-NPs or other structures.

4 Conclusions

Porous HoMSs Co_3O_4 samples with specified shell numbers(single-, double-, triple-, and quadruple-, respectively) were synthesized by the sequential-template method. Profiting from the superiorities of inimitable porous ball in ball structure, HoMSs Co_3O_4 exhibited as an excellent electrode materials for supercapacitors. The specific capacitances of the 3S-HoMSs that possessed the largest specific surface area and the thinnest wall achieved 688.2 F/g at a current density of 0.5 A/g and 89.8% still maintained even under a high current density up to 10 A/g. It's worth noting that the electrode with 3S-HoMSs also showed excellent cycle stability(93.2% remained after 2000 cycles at 2 A/g). It can be sure that accurately controlled synthesis of functional materials with e hollow structure will guide e supercapacitors with lower cost and better performance.

Electronic Supplementary Material

Supplementary material is available in the online version of this article at http://dx.doi.org/10.1007/s40242-019-0040-3.

References

[1] AraveLeela M. R., Gowda S. R., Shaijumon M. M., Ajayan P. M., *Adv. Mater.*, **2012**, *24*, 5045

[2] Xu Y., Wang X., An C., Wang Y., Jiao L., Yuan H., *J. Mater. Chem. A*, **2014**, *2*, 16480

[3] Ke Q., Tang C., Yang Z., Zheng M., Mao L., Liu H., Wang J., *Electrochim. Acta*, **2015**, *163*, 9

[4] Peng S., Li L., Tan H., Cai R., Shi W., Li C., Mhaisalkar S. G., Srinivasan S., Ramakrishna S., Yan Q., *Adv. Funct. Mater.*, **2014**, *24*, 2155

[5] Wang G., Zhang L., Zhang J., *Chem. Soc. Rev.*, **2012**, *41*, 797

[6] Tang H., Wang J., Yin H., Zhao H., Wang D., Tang Z., *Adv. Mater.*, **2015**, *27*, 1117

[7] Zhang L., Zhao X., *Chem. Soc. Rev.*, **2009**, *38*, 2520

[8] Chen S., Ramachandran R., Mani V., Sarawathi R., *Int. J. Electrochem. Sci.*, **2014**, *9*, 4072

[9] Rakhi R. B., Chen W., Cha D., Alshareef H. N., *Nano Lett.*, **2012**, *12*, 2559

[10] Yuan C., Yang L., Hou L., Shen L., Zhang X., Lou X., *Energy Environ. Sci.*, **2012**, *5*, 7883

[11] Fan H., Quan L., Yuan M., Zhu S., Wang K., Zhong Y., Chang L., Shao H., Wang J., Zhang J., Cao C., *Electrochim. Acta*, **2016**, *188*, 222

[12] Yan J., Wang Q., Wei T., Fan Z., *Adv. Energy Mater.*, **2013**, *4*, 1

[13] Simon P., Gogotsi Y., *Nat. Mater*., **2008**, *7*, 845

[14] Wang D., Wang Q., Wang T., *Inorg. Chem.*, **2011**, *50*, 6482

[15] Wang X., Li M., Chang Z., Yang Y., Wu Y., Liu X., *ACS Appl. Mater. Inter.*, **2015**, *7*, 2280

[16] Yu X., Yu L., Wu H., Lou X., *Angew. Chem., Int. Ed*., **2015**, *54*, 5331

[17] Xia X., Tu J., Mai Y., Wang X., Gu C., Zhao X., *J. Mater. Chem.*, **2011**, *21*, 9319

[18] Zhang Y., Wang Y., Xie Y., Cheng T., Lai W., Pang H., Huang W., *Nanoscale*, **2014**, *6*, 14354

[19] Du H., Jiao L., Wang Q., Yang J., Guo L., Si Y., Wang Y., Yuan H., *Nano Res.*, **2013**, *6*, 87

[20] Chen Y., Li Z., Lou X., *Angew. Chem.*, *Int. Ed.*, **2015**, *54*, 10521

[21] Wang J., Tang H., Ren H., Yu R., Qian J., Mao D., Zhao H., Wang D., *Adv. Sci.*, **2014**, *1*, 1400011

[22] Guo J., Yin Z., Zang X., Dai Z., Zhang Y., Huang W., Dong X., *Nano Res.*, **2017**, *10*, 405

[23] Zhao X., Yu R., Tang H., Mao D., Qi J., Wang B., Zhang Y., Zhao H., Hu W., Wang D., *Adv. Mater.*, **2017**, *29*, 1700550

[24] Chen M., Wang J., Tang H., Yang Y., Wang B., Zhao H., Wang D., *Inorg. Chem. Front.*, **2016**, *3*, 1065

[25] Park G. D., Lee J. H., Lee J. K., Kang Y. C., *Nano Res.*, **2014**, *7*, 1738

[26] Lai X., Halpert J. E., Wang D., *Energy Environ. Sci*., **2012**, *5*, 5604

[27] Wang J., Yang N., Tang H., Dong Z., Jin Q., Yang M., Kiisailus D., Zhao H., Tang Z., Wang D., *Angew. Chem., Int. Ed.*, **2013**, *125*, 6545

[28] Dong Z., Ren H., Hessel C. M., Wang J., Yu R., Jin Q., Yang M., Hu Z., Chen Y., Tang Z., Zhao H., Wang D., *Adv. Mater.*, **2014**, *26*, 905

[29] Wang J., Wan J., Wang D., *Acc. Chem. Res.*, **2019**, *52*, 2169

[30] Xu S., Hessel C. M., Ren H., Yu R., Jin Q., Yang M., Zhao H., Wang D., *Energy Environ. Sci.*, **2014**, *7*, 632

[31] Salhabi E., Zhao L., Wang J., Yang M., Wang B., Wang D., **2019**, *58*, 9078

[32] Lai X., Li J., Korgel B. A., Dong Z., Li Z., Su F., Du J., Wang D., *Angew. Chem., Int. Ed.*, **2011**, *123*, 2790

[33] Lou X., Deng D., Lee J., Feng J., Archer L., *Adv. Mater.*, **2008**, *20*, 258

[34] Kinsinger N. M., Dudchenko A., Wong A., Kisailus D., *ACS Appl. Mater. Interfaces*, **2013**, *5*, 6247

[35] Xiong S., Yuan C., Zhang X., Xi B., Qian Y., *Chem. Eur. J.*, **2009**, *15*, 5320

[36] Deng S., Xiao X., Xing X., Wu J., Wen W., Wang Y., *J. Mol. Catal. A: Chem.*, **2015**, *398*, 79

[37] Xu J., Gao P., Zhao T., *Energy Environ. Sci.*, **2012**, *5*, 5333

[38] Wang L., Liu X., Wang X., Yang X., Lu L., *Curr. Appl. Phys.*, **2010**, *10*, 1422

[39] Zhang F., Yuan C., Lu X., Zhang L., Che Q., Zhang X., *J. Power Sources*, **2012**, *203*, 250

[40] Pal M., Rakshit R., Singh A. K., Mandal K., *Energy*, **2016**, *103*, 481

[41] Fan M., Ren B., Yu L., Song D., Liu Q., Liu J., Wang J., Jing X., Liu L., *Electrochim. Acta*, **2015**, *166*, 168

[42] Liu X., Gao Y., Yang G., *Nanoscale*, **2016**, *8*, 4227

[43] Wang Y., Pan A., Zhu Q., Nie Z., Zhang Y., Tang Y., Liang S., Cao G., *J. Power Sources*, **2014**, *272*, 107